Measuring Electronic Coupling in the Reaction Center of Purple Photosynthetic Bacteria by Two-Color, Three-Pulse Photon Echo Peak Shift Spectroscopy

Dilworth Y. Parkinson, Hohjai Lee, and Graham R. Fleming*

Department of Chemistry, University of California, Berkeley and Physical Biosciences Division, Lawrence Berkeley National Laboratory, Berkeley, California 94720

Received: January 2, 2007; In Final Form: April 5, 2007

One- and two-color, three-pulse photon echo peak shift spectroscopy (1C and 2C3PEPS) was used to estimate the electronic coupling between the accessory bacteriochlorophyll (B) and the bacteriopheophytin (H) in the reaction center of the purple photosynthetic bacterium *Rhodobacter sphaeroides* as $\sim 170 \pm 30$ cm^{-1}. This is the first direct experimental determination of this parameter; it is within the range of values found in previously published calculations. The 1C3PEPS signal of the Q_y band of the bacteriochlorophyll B shows that it is weakly coupled to nuclear motions of the bath, whereas the 1C3PEPS signal of the Q_y band of the bacteriopheophytin, H, shows that it is more strongly coupled to the bath, but has minimal inhomogeneous broadening. Our simulations capture the major features of the data with the theoretical framework developed in our group to separately calculate the response functions and population dynamics.

Introduction

The reaction center (RC) of purple photosynthetic bacteria converts the energy of sunlight to chemical charge separation with a quantum yield of nearly 100%.[1−3] Six chromophores are involved (see Figure 1): two facing bacteriochlorophylls form the special pair (P); an accessory bacteriochlorophyll flanks P on each side (B_A and B_B); and adjacent to each B is a bacteriopheophytin (H_A and H_B).[4] In addition, a quinone molecule sits near each H (Q_A and Q_B). Energy transfer occurs from H to B to P, and electron transfer takes place from P toward H_A, then to Q_A and Q_B.[2]

Because the various chromophores are in such close proximity (5−10 Å), they influence each other. For example, there is significant mixing between the electronic states of the chromophores, and this contributes to the speed and efficiency of energy and electron transfer in the RC. Another manifestation of the mixing is the distinctive Q_y region of the absorption spectrum, displayed in Figure 2. The 750, 800, and 860 nm bands are labeled H, B, and P, describing which chromophore makes the dominant contribution to each band. But these labels do not give a full description of the character of the states, because each spectral band is actually a mixed band with contributions from multiple chromophores.[5−18] For example, the two molecules which form P strongly couple to form two new exciton states: the lower one (P_-) absorbs at 860 nm, labeled P in Figure 2, whereas the upper one (P_+) gives rise to a band that is not clearly resolved between 810 and 835 nm.[19]

Various experimental and theoretical efforts have been made to quantitatively determine the magnitude of the coupling between various chromophores in the reaction center, but this has been difficult. The splitting observed in the absorption spectrum cannot be used alone, because the "original" positions of the bands are not known, and in addition, the observed spectral bands are superpositions of A-side and B-side chromophores. For example, the main 800 nm peak corresponds to B_A, but the shoulder at 810 nm corresponds to B_B.[19,20] One approach to determine the coupling from the absorption spectrum while avoiding these problems is to use mutants in which pigments are exchanged or deleted, but because of the changes in the RC this technique introduces, this has resulted only in qualitative results.[21] The main experimental approach used to experimentally determine the coupling has been to deduce coupling values on the basis of the time scales of energy and electron transfer.[22−24]

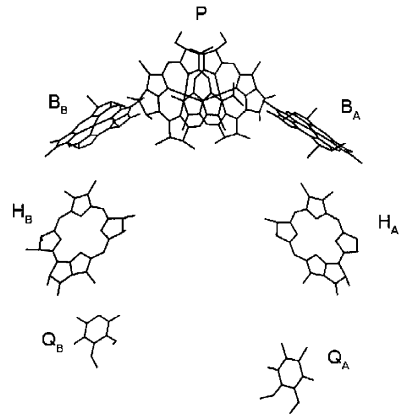

Figure 1. The chromophores of the reaction center of *Rb. sphaeroides*: the special pair of bacteriochlorophylls (P), accessory bacteriochlorophylls (B), bacteriopheophytins (H), and quinones (Q). Structure 1PCR from the Protein Data Bank.[4]

We recently demonstrated that two-color, three-pulse photon echo peak shift (2C3PEPS) provides direct experimental access to the strength of electronic coupling in an excitonically coupled dimer.[25] In these homodimers, the excited electronic states become mixed so that a nuclear fluctuation that affects either of the chromophores appears as a correlated shift in the energies of both of the exciton states. 2C3PEPS is sensitive to this kind of correlation between spectral regions. Because the extent of correlation in the fluctuations of the exciton states is dependent on the strength of the coupling between the two chromophores,

* To whom correspondence should be addressed. E-mail: GRFleming@lbl.gov.

10.1021/jp070029q CCC: $37.00
Published on Web 05/26/2007

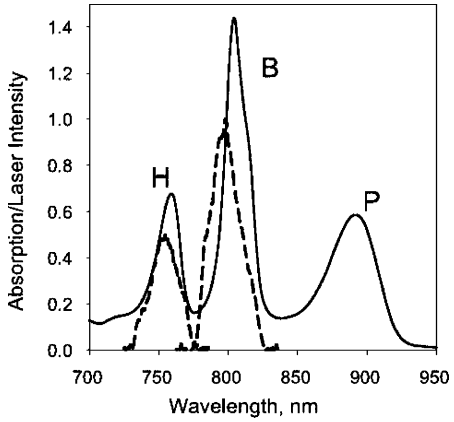

Figure 2. Absorption spectrum of the RC at 77 K (solid lines), with bands labeled according to the dominant contributing chromophore; the spectra of the two colors of laser pulses used in the experiments (dashed lines).

2C3PEPS can accurately measure the value of the coupling without knowing the original site energies of the two chromophores.[26,27] The information content of the 2C3PEPS experiment is that of a cross-peak in a two-dimensional experiment, although 2C3PEPS lacks the phase information present in a two-dimensional experiment.

Although not as strongly coupled as the special pair, the B and H chromophores are significantly coupled to each other. The states observed in the absorption spectrum correspond to mixtures of B and H. Theoretical calculations based on the dipole−dipole approximation indicate that the value for the electronic coupling between nearest neighbor B and H chromophores lies in the range of 100−200 cm^{-1}.[5−18] The purpose of this study is to make a direct experimental measurement of this parameter.

Experimental Methods

His-tagged *Rhodobacter sphaeroides* cells were supplied by the Boxer lab. Cells were grown and reaction centers were purified according to their published protocol.[28] Briefly, cells were grown semiaerobically in the dark. Cells were disrupted with a French press, and reaction centers were solubilized with the detergent lauryldimethylamine oxide (LDAO). Purification was carried out with a nickel−NTA column followed by a DEAE column. Our yield and purity were similar to their published values. After concentration of the sample, sodium ascorbate was added (∼100 mM) to prereduce Q_A. The samples were diluted with 60% glycerol and placed in a 0.2 mm quartz cell. Under these conditions, the optical density at 800 nm was 0.1−0.3. Experiments were performed at 77 K using an Optistat DN cryostat from Oxford Instruments. To test the integrity of our sample, one-color, 800 nm transient absorption experiments were periodically carried out before and after collection of other data, and we found that this data was consistent with the literature.

The photon echo experiment[29−31] is carried out by focusing the three pulses, arranged in equilateral triangle geometry, onto the sample with a 20 cm singlet lens. Integrated echo profiles are measured as a function of the coherence time (the period between the first two pulses) for fixed values of the population time (the period between the second and third pulses). The peak shift for a given population time is the value of the coherence time that gives the maximum signal, as determined by fitting to a single Gaussian function.

The B and H spectral bands are centered at 800 and 760 nm, respectively, and colors for the laser pulses were chosen to correspond to these two bands. For the one-color experiments, all three pulses are of the same color. For the two-color experiments, the first two pulses are set to the "pump" wavelength, while the third pulse is set to the "probe" wavelength. We carried out one-color experiments at both 750 and 800 nm and two-color experiments with both the 750 and 800 nm pulses as the pump color ("downhill" and "uphill" experiments, respectively) with the other color as the probe. We will refer to the four experiments as 1C 750, 1C 800, 2C downhill, and 2C uphill. As shown in previous theoretical work, in order to determine the degree of mixing in this type of system, peak shifts at all four color combinations are needed.[27] The integrated photon echo signal is collected on PMTs in two phase-matched directions. For the two-color experiments, 25 nm bandwidth filters corresponding to the probe wavelength were placed in front of the PMTs to prevent scattering from the pump beams. Data were collected using an optical chopper and lock-in amplifiers.

Laser pulses were produced by a home-built amplifier seeded by a Femtosource Compact Pro Ti:Sapphire oscillator (Femtolasers, Inc.). This system produces ∼40 fs pulses, centered at ∼800 nm, at 1 kHz. Part of this beam was used directly for the experiments, while ∼5 mW was used to pump an optical parametric amplifier (Coherent 9450) to produce ∼40 fs pulses centered at 750 nm. Optical filters centered at 750 and 800 nm with bandwidths of 25 nm were used in the experiments to prevent undesired spectral overlap between the beams and to improve day-to-day reproducibility of the pulse shapes. The exception was the 1C 750 experiment, in which razor blades in the prism compression line were used to control the bandwidth (this was done to increase the available pulse power in this experiment). The spectra of the laser pulses are shown in Figure 2; note the minimal spectral overlap between the pulses, that each pulse overlaps with most of the corresponding spectral band, and that each pulse has negligible overlap with the other spectral band. The final pulse energies on the sample were 1−5 nJ/pulse.

Theoretical Considerations

Yang and Fleming[26] (YF) have described the theoretical basis for understanding both one- and two-color photon echo peak shifts for a strongly coupled homodimer. This theory was extended by Mancal and Fleming[27] (MF) for application to heterodimers. Their work showed how the electronic mixing between the two monomers could be determined by measuring the one- and two-color peak shifts in the long population time limit (after ∼100 fs). We briefly summarize their work here.

In an excitonically coupled dimer, excited states of each monomer, with energies ϵ_a and ϵ_b, respectively, are mixed to form two new exciton states, an upper state (μ) and a lower state (ν), which correspond to the observed spectral bands. The degree of mixing is described by the mixing angle, θ, according to the equation

$$\tan(2\theta) = \frac{2J}{\epsilon_a - \epsilon_b} \tag{1}$$

where J is the coupling between the monomers.

Because μ and ν are exciton states that contain contributions from both of the original monomer states, any nuclear motions associated with one of the monomers causes correlated fluctuation in both μ and ν. The 2C3PEPS signal is sensitive to this

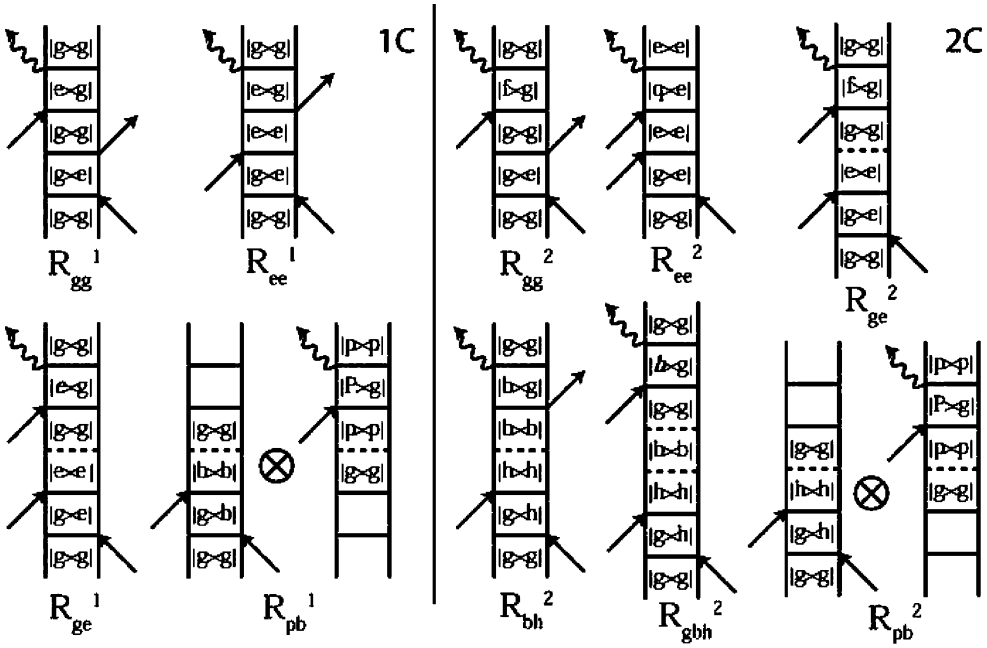

Figure 3. Feynman diagrams for the one-color (1C), left, and two-color (2C), right, experiments. See text for details.

correlation. The coupling coefficient, $C_{\mu\nu}$, is the critical parameter that relates the experiment to the coupling. MF showed that for a heterodimer system with no energy transfer and in which the chromophores have independent baths, the experimental coupling coefficient (C_{τ^*}) is found from the one- and two-color peak shifts,

$$C_{\mu\nu} = 2\sin^2\theta\cos^2\theta \approx C_{\tau^*} = \frac{\tau^*_{\mu\nu}(T)}{\tau^*_{\mu\nu}(T) + \frac{1}{2\kappa}(\tau^*_{\mu}(T) + \tau^*_{\nu}(T)\kappa^3)} \quad (2)$$

where $\kappa = \tau^*_{\mu\nu}(T)/\tau^*_{\nu\mu}(T)$. In this equation, $\tau^*_{\mu}(T)$ and $\tau^*_{\nu}(T)$ represent the one color peak shift on the upper and lower exciton states, respectively, and $\tau^*_{\mu\nu}(T)$ and $\tau^*_{\nu\mu}(T)$ represent the downhill and uphill peak shifts, respectively. The peak shifts are a function of the population time, T.

To determine the electronic coupling, J, from C_{τ^*}, we could use the following equation based on the difference in energy between the two exciton states:

$$E_\mu - E_\nu = 2J\sqrt{1 + (1/\tan(2\theta))^2} \quad (3)$$

Up to this point, we have discussed the theoretical framework for a system with no population dynamics. Obviously, this will not be sufficient to describe the RC. To include the dynamics, we will use the approach developed by YF for energy transfer and reactive systems.[32−34] In implementing this approach, we make three simplifying assumptions. First, we assume that the population dynamics can be separated from the nuclear dynamics; this assumption is often justified, but partially breaks down in this case because the energy transfer is so fast. Second, we assume that there is no correlated energy transfer due to static inhomogeneity;[33,35] this is justified in our case because of the small inhomogeneity in the spectral bands (as will be shown by the 1C3PEPS data). Third, we assume that we can ignore the effect of nuclear dynamics associated with energy transfer, or in other words, that all phase information is lost upon energy transfer.[36]

The peak shift is less sensitive to population dynamics than other techniques, so simulations with a number of population dynamics schemes with a range of time scales could be used to give satisfactory fits. Thus, the population dynamics used in our simulations are based on the literature.[13−15,19,22,37−56] Energy transfer from H_A to B_A or H_B to B_B occurs on a 50 fs time scale. Energy transfer from B_B and B_A to P_+ takes place on a 175 fs time scale. Internal conversion from P_+ to P_- occurs on a 75 fs time scale. Charge separation from P_- to $P^+B_A^-H_A$ then to $P^+B_AH_A^-$ takes place on 2 and 1 ps time scales. We tested the effect of including direct charge transfer from B or H in our simulations,[46,49−52,57] but again, these changes in the population dynamics had only a small effect on the peak shift, so we did not include them in most of our simulations. We include two characteristics of the system in our simulations: first, after charge separation to $P^+B_AH_A^-$, the B_A band undergoes an electrochromic blue shift of $\sim$300 cm^{-1}; second, when B_A or H_A carries a charge, the corresponding band is bleached. For the experiments in which the first two pulses are at 800 nm, we assume that we excite 75% B_A and 25% B_B because of the location of the spectra and because this yields good fits. For similar reasons, in the experiments in which the first two pulses are at 750 nm, we assume that we excite H_A and H_B equally.

To implement the simulations, we use the response function formalism, in which a number of possible pathways are added together to determine the overall response of the system to the laser pulses.[58−60] Because of population dynamics, different pathways will contribute to the signal with different magnitudes at each time in the experiment. We assume that the 750 nm pulse interacts only with the H band, and the 800 nm pulse interacts with the B band, the B band after its electrochromic shift due to electron transfer, and with P_- through an excited-state absorption which, at 77 K, we assume is centered at 810 nm.[19] We neglect interaction with the P_+ state (centered between 810 and 835 nm) because of its relatively small transition dipole moment and the small population that builds up on it.

Each pathway that can give rise to a signal is represented by a Feynman diagram; those used for our simulations are shown in Figure 3. In the diagrams, the arrows represent the three

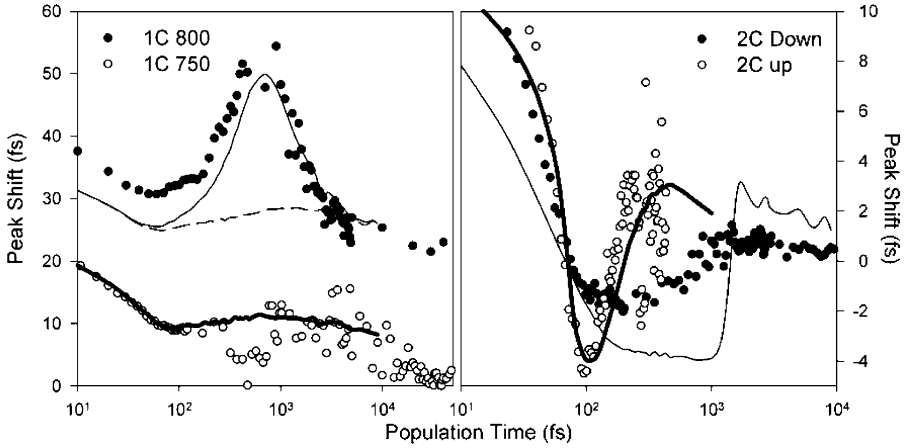

Figure 4. Peak shift plots for RCs at 77 K. (left) Open circles and thick solid line are experimental and simulated 1C 750-nm peak shifts. Filled circles and thin solid line are experimental and simulated 1C 800-nm peak shifts; the dashed line is simulated 800-nm peak shift without the excited-state absorption from P_-. (right) Filled circles and thin line are experimental and simulated 2C downhill peak shift signals. Open circles and thick line are experimental and simulated 2C uphill peak shift signals.

pulses, and the letters in the diagrams represent the electronic states through which the system can pass: ground (g), B (b), H (h), P_- (p), the B/H two-exciton state (q), and the two-exciton state corresponding to excited-state absorption from P_- (P). In one-color diagrams that could correspond to either the 800 or 750 nm experiments, an e is used to represent either B or H, depending on the experiment. In two-color diagrams, for the uphill (downhill) experiments, an e is used to represent B (H), and an f is used to represent H (B). An italic *e* or *b* denotes that the interaction will be different after formation of $P^+B_AH_A^-$ due to the electrochromic shift of the B_A band.

The left-hand side of Figure 3 shows the diagrams used in the one-color simulations. In these diagrams, all three pulses are of the same color. R_{gg}^1 and R_{ee}^1 correspond to pathways in which no energy or electron-transfer takes place; these diagrams are the two diagrams normally used to describe a two-level system. R_{ge}^1 corresponds to the pathway in which B (or H) is excited, followed by energy transfer that returns B (H) to its ground state, followed by re-excitation, either to the original excited state or, in the case of B, to its electrochromically shifted excited state if electron transfer to $P^+B_AH_A^-$ has taken place. R_{ge}^1 can also be used to describe direct electron transfer from B_A to $P^+B_A^-H_A$, followed by electron transfer to $P^+B_AH_A^-$. R_{pb}^1 applies only to the 800 nm experiment and corresponds to the case in which B is excited, and this excitation energy is transferred (through P_+) to P_-, from which there is an excited-state absorption to a two-exciton state.[22]

The right-hand side of Figure 3 shows the six diagrams used in the two-color simulations. In these diagrams, the first two pulses correspond to one color, and the third pulse is of the other color. R_{gg}^2 and R_{ee}^2 correspond to the case without energy or electron transfer, in which the first two pulses interact with B (H) and the third pulse interacts with H (B). These are the diagrams used by YF and MF in their simulations of strongly coupled dimers. R_{ge}^2 applies to RCs that interact with the third pulse after the population has moved away from B (or H).

The other three diagrams apply to the downhill experiment only and correspond to the excitation of H by the first two pulses. For R_{bh}^2, this is followed by energy transfer to B, followed by interaction with the third pulse. For R_{gbh}^2, this is followed by energy transfer to B and then subsequent energy or electron transfer, or both, away from B, followed by interaction of the third pulse with B. For R_{ph}^2, this is followed by energy transfer to B, then P_+, then P_-, followed by an excited-state absorption from P_-.

Results

The 1C 800 transient grating signal (not shown) decays on a 90 fs time scale to ~10% of the maximum value before rising to higher value on a 3 ps time scale. The rise lasts until ~10 ps, at which point the signal stays approximately constant until the end of our data collection (100 ps). The 1C 800 peak shift decay is shown as the filled circles in the left panel of Figure 4. It begins at ~45 fs at zero population time and decays to ~30 fs on a sub-50 fs time scale, reaching a local minimum at ~60 fs. It then rises, peaking at a population time of ~700 fs before falling again. From ~3 ps, the peak shift decays on a longer time scale (~30 ps), nearly reaching its terminal peak shift of ~20 fs by a population time of ~50 ps. The magnitude and exact time scales of the rise and fall of the bump feature varied because at the corresponding population times, there is a local minimum in the transient grating data, which means there is a very small signal from which to determine the peak shift.

The 1C 750 transient grating signal (not shown) decays on a time scale of 50 fs to a value near zero before rising very slightly on a 3 ps time scale. The 1C 750 peak shift signal is shown as the open circles in the left-hand panel of Figure 4. It begins at 25 fs and decays to ~9 fs on a sub-50 fs time scale before decaying to zero on a longer time scale, which is difficult to determine because of the noise in the data. The reason the peak shift becomes noisy is that at that time, as in the 1C 800 case, the transient grating (and the corresponding signal that gives rise to the peak shift determination) has become very small. It should be noted that the fact that the signal goes to zero does not mean that the peak shift is zero; rather, it simply means we cannot determine the peak shift.

The 2C downhill transient grating signal (not shown) rises on a 100 fs time scale before decaying on a 220 fs time scale. Although these time scales are longer than the time scales in the other data sets, we find that the same parameters for the population dynamics allow us to fit the data satisfactorily. As in the 1C 800 case, the decay reaches a finite offset before rising on a ~3 ps time scale and leveling off after ~10−20 ps.

The 2C downhill peak shift signal is shown as the filled circles in the right-hand panel of Figure 4. It begins at ~15 fs, but the uncertainty in this value is large (±5 fs) because of the uncertainty in time zero (which is difficult to set in two-color experiments)[31] and the fact that the peak shift is rapidly changing in that region. The peak shift decays on two time scales: a sub-50 fs time scale and an ~500 fs time scale. A unique aspect of

the 2C downhill peak shift is that it goes to negative values, crossing zero at ~75 fs before reaching a minimum of approximately −2 fs at a population time of 200 fs. This is followed by a rise; the peak shift becomes positive at ~1 ps, and reaches a maximum of 1 fs before decaying very slightly. It should be noted that the peak shift crosses from negative to positive at the point where the transient grating reaches its minimum.

The 2C uphill transient grating signal (not shown) decays on a 120 fs time scale, and there is no observed rise. The 2C uphill peak shift is shown as the open circles in the right-hand panel of Figure 4. The peak shift starts at ~15 fs, although this value again has a relatively large uncertainty (±5 fs) for the same reasons as the initial 2C downhill peak shift. The peak shift decays on a sub-50 fs time scale, reaching a minimum of −2 fs around a population time of 100 fs. It then rises to a value of ~2 fs at 300 fs before leveling off. After ~500 fs, the data becomes too noisy to fit (again, due to the decay of the signal to zero).

Discussion

The main purpose of our experiments is to determine the coupling between B and H, but before discussing our measurement of this parameter in detail, we will first analyze the major features of each data set individually. Our ability to understand and simulate the data will give us confidence in our estimates of the electronic coupling.

The 1C 800 transient grating and peak shift experiments performed at 273 K have been previously reported by Groot et al.[61] Our transient grating data is in good agreement with that work, and our simulations confirm their interpretation of its features. We performed simulations including alternate charge separation pathways and found that the offset after the initial decay does increase with an increase in direct B-to-H charge separation; our simulations show that the transient grating would decay to near zero without a contribution from direct B^*H to B^+H^- charge separation.

After fixing the population dynamics on the basis of literature values and our transient grating data, the two variable parameters in the 1C 800 peak shift simulations were the B−H coupling and the line-broadening function, $g(t)$; the simulation is shown as the thinner solid line in the left-hand panel of Figure 4. We opted to use a simple $g(t)$, with a 60 fs Gaussian with 25 cm^{-1} of coupling and an inhomogeneous width of 45 cm^{-1}. To model the slow decay of the peak shift we see on a ~30 ps time scale, we include an additional 30 ps exponential mode with 15 cm^{-1} of coupling. Our decision not to include specific vibrational modes in our simulations was based mainly on the fact that these modes were not necessary for a satisfactory fit of the data.

Our observed 1C 800 peak shift is very large over the whole time range. This can be attributed to three factors. First is the presence of inhomogeneous broadening present in the B band, which leads to a large peak shift at long times relative to the peak shift at time zero. Resonance Raman experiments[62] and the 273 K work by Groot et al. report an inhomogeneous width of 55 cm^{-1}; we use 45 cm^{-1}. Second, the overall coupling to the bath is quite small, which leads to a large initial peak shift. Third, as previous experiments have shown, peak shifts are generally larger at lower temperatures, and the temperature dependence is greater for systems that are weakly coupled to the bath, as in this case.[63−65]

We included a 30 ps exponential component in our line-broadening function because we see a small decay on a long time scale (between population times of ~10 and 100 ps, the peak shift decays by ~3 fs; in the 273 K data, it decays by ~1 fs over this time). On the basis of our population dynamics scheme (and in accordance with our transient grating data), the population dynamics occurring during this time period would make a very small contribution. Previous studies have assigned changes occurring on this time scale to protein relaxation that takes place after charge separation.[48,54,55]

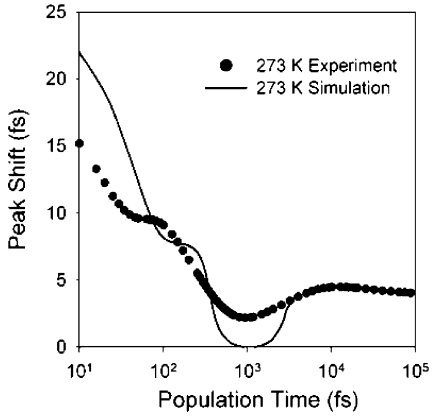

Figure 5. 1C 800-nm peak shift data at 273 K. Filled circles are the fit to the data of Groot et al.[61] Solid line is our simulation of the data.

We attribute the maximum in our data to interference between the pathways involving B and the pathway involving excited-state absorption from P_-. The excited-state absorption pathway, which is a free induction decay signal centered at a coherence time of zero, is subtracted from the other pathways, which are centered at positive coherence times. This increases the value of the coherence time that gives the greatest signal, increasing the peak shift.

To confirm our assignment of the maximum in the 77 K data to interference from the excited-state absorption from P_-, we show a simulation of the peak shift signal without the excited-state absorption term (the dashed line in the left-hand panel of Figure 4). The prominent maximum seen in the data (filled circles) and in the full simulation (solid thin line) disappears when the excited-state absorption pathway is removed (dashed line). An additional point in support of the attribution of the maximum to the excited-state absorption from P_- is that the relative population on P_- as a function of population time closely tracks the rise and fall in the peak shift.

Because of the large difference between our data and the previously published peak shift, we felt it was important to carry out a simulation of the 273 K data. We used the same line-broadening function as in our low-temperature simulations (recalculated for the higher temperature). Groot et al. used a line-broadening function that included vibrations with a specific set of phases with respect to each other in order to fit the plateau they observed after a fast 50 fs decay. In our simulation of their data, this plateau appears due to population dynamics. Although the population dynamics is known to be slightly temperature-dependent, for simplicity, we held these parameters constant, which introduces some error in our simulation. The change we did make in the simulations between the two temperatures was to shift the energy of the P_- band of the excited-state absorption, corresponding to the shift in the P_- band in the absorption spectrum between the two temperatures (~350 cm^{-1}). As can be clearly seen by comparing our simulations of the 1C 800 peak shift at 77 K (the thin solid line in the left-hand panel of Figure 4) and 273 K (the solid line in Figure 5), this change has an enormous effect on the appearance of the simulated peak shift. Because of the shift in wavelength of the excited-state absorption, this pathway interferes differently with the other

pathways, leading to a dip in the peak shift rather than a bump. The higher temperature naturally leads to a significantly lower terminal peak shift. Thus, although the appearance of the two peak shifts is qualitatively very different, they can both be understood on the basis of the same set of parameters.

The 1C 750 peak shift is very different from that of the 1C 800 peak shift. Our simulation of the 1C 750 peak shift is the thicker solid line in the left-hand panel of Figure 4. To construct the $g(t)$, we used a 60 fs Gaussian with 85 cm^{-1} of coupling, a 30 ps exponential with 85 cm^{-1} of coupling, and no inhomogeneous broadening. The observed absence of inhomogeneous broadening in H is in line with the small inhomogeneity seen in hole-burning experiments.[66] The differences between the peak shift of the H and B bands may be due to differences in the environments of the chromophores as well as inherent differences between the chromophores. Bacteriopheophytin lacks a central metal atom, making it more flexible than bacteriochlorophyll. The greater flexibility of H may be why it is more strongly coupled to the environment, leading to the smaller values of the peak shift at all population times.

We now turn to the two-color data. Recalling that we have introduced population transfer into the YF and MF models in an ad hoc way that does not allow memory conservation and neglects pulse duration and quantum effects, we expect to be more successful in modeling the uphill data than the downhill data. The uphill signal includes contributions from only three response functions, of which two (R_{gg}^2 and R_{ee}^2) are the same pathways as used in the MF model. Additionally, only the decay of the B population contributes to the calculation. In contrast, the downhill data have both population feeding and decay, and will require a model that properly accounts for finite pulse duration effects. Such a model incorporating time-nonlocal, non-Markovian dynamics, which allows the self-consistent inclusion of coherence transfer, is under development, and application to the reaction center will be presented elsewhere.[67]

To simulate the 2C downhill and uphill peak shifts, we used the same population dynamics schemes as the 1C 750 and 800 peak shift simulations, respectively. In addition, the $g(t)$'s used were taken from those determined during fitting of the 1C data. We follow the method of MF[27] for a heterodimer, using the $g(t)$'s of the two chromophores to form an average and a difference $g(t)$. The qualitative expectations described above are borne out by the fits shown in Figure 4: the uphill data are well described by the model, and the downhill data are qualitatively modeled, but the quantitative agreement is poor. Because of the decay of the 2C uphill transient grating signal to near zero in <1 ps, we could collect accurate peak shift data only to $\sim$500 fs. The main feature we observe before our 500 fs cutoff is a dip around 100 fs. Our simulations indicated that this is due to the competing effects of the two response functions, which are related to the decay of the B population. The first is R_{ee}^2, which decays with the decay of the population on B. The second is R_{ge}^2, which grows in with the decay of the population from B. The former (decaying) pathway gives rise to a negative peak shift whereas the latter pathway gives rise to a positive peak shift. The dip in the 2C uphill peak shift occurs at the location at which there is a crossover between the contributions of these two pathways.

A negative region (from 75 fs to $\sim$1 ps) of the 2C peak shift is also apparent in the downhill data and arises from the same effect: very rapid population dynamics can overshadow the effect of dephasing on the peak shift. This latter effect would be expected to generate only positive peak shifts, but when the overall signal is decaying very rapidly as a function of population time, the signal from negative coherence times can be larger than those at positive coherence times. This explanation of the negative peak shift is confirmed by the rise in the peak shift to positive values at a population time near 1 ps. This rise occurs precisely at the point when the slope of the transient grating changes from negative to positive. At this point, the effect that was previously pushing the peak shift negative is no longer present.

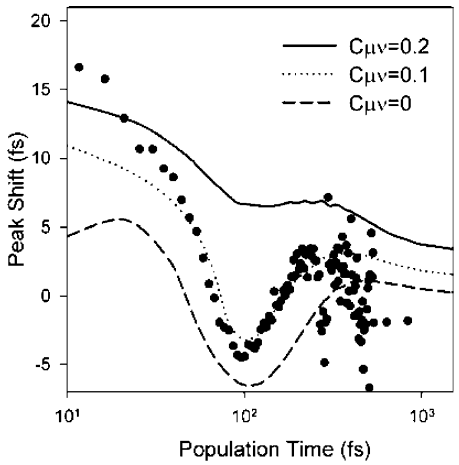

Figure 6. Experimental 2C uphill peak shift signal (filled circles) and simulations for three values of $C_{\mu\nu}$: 0 (dashed), 0.1 (solid), and 0.2 (dotted).

We now turn to a discussion of the coupling coefficient, $C_{\mu\nu}$. The reaction center is significantly more complex than the dimeric model systems without population dynamics that were studied by YF and MF, and the ratio given by eq 2 changes significantly over the time during which we have data, so in this case, it cannot be used to determine $C_{\mu\nu}$. An approach that can be used to determine $C_{\mu\nu}$ in this case is to fit the 2C uphill peak shift. This approach is justified when $C_{\mu\nu}$ is expected to be small. In this situation, the individual one-color peak shift experiments can be used to obtain good approximations to the line-broadening function of the two individual chromophores, and either one of the two-color peak shift experiments can then be used to determine the coupling. In this case, the 2C uphill experiment is preferable to the 2C downhill experiment for use in determining $C_{\mu\nu}$ because it is influenced less by the population dynamics and, as noted above, is closer to the model systems studied by YF and MF.

Figure 6 shows a series of three simulations of the 2C uphill peak shift carried out with all parameters held constant except the value of the B−H coupling coefficient, which is set to 0, 0.1, and 0.2. It is evident from this plot that $C_{\mu\nu} = 0.1$ gives the best agreement with experiment. The general trend that can be seen in these simulations is the same as that observed by YF[26] and MF:[27] as $C_{\mu\nu}$ is increased, the peak shift at essentially all population times is also increased. This same trend was observed in coupling-dependent simulations of the other three peak shifts. We believe this is true because although the pathways that contribute to the signal in these cases are not the same as those for a system without energy transfer, the pathways that do contribute to the signal still depend on $C_{\mu\nu}$.

As described in Theoretical Considerations, we can use the value of $C_{\mu\nu}$ to determine the value of the B−H electronic coupling using our knowledge of the energies of the two mixed exciton levels. Using 750 cm^{-1} as the difference between these levels (based on the absorption spectrum) gives a value of $J =$ 170 cm^{-1}. The range of values given in the literature is $\sim$100−200 cm^{-1}.[5−18] To give an idea of the error associated with this

value, we note that values of $C_{\mu\nu}$ of 0.05 and 0.15 would correspond to coupling values of 130 and 200 cm^{-1}, respectively. We therefore assign an uncertainty of ± 30 cm^{-1} to our result. To give a frame of reference for the relative magnitude of this coupling, we note that theoretical calculations put the coupling between the two bacteriochlorophylls that make up the special pair between 400 and 1000 cm^{-1}.[5−18]

Concluding Remarks

Through 1C and 2C peak shift measurements on the B and H bands of the RC, we estimated that the B−H coupling is 170 $\pm$ 30 cm^{-1}. The simulations and analysis used are clearly oversimplified and represent a first attempt at using two-color photon echo spectroscopy to provide quantitative experimental values for electronic couplings. Methods for calculating echo signals that self-consistently include the quantum dynamics and optical interactions of multichromophore systems are under development, and we believe the success of the preliminary efforts reported here is sufficient to encourage further experiments and complementary theory. One interesting question that this study did not address is the asymmetry in the reaction center, which results in electron transfer from P to H_A but not H_B. The degree to which differences in electronic coupling between charge transfer states on the two sides of the RC determine this asymmetry has been the subject of extensive research and is still not a settled question. Although the measured coupling between the B and H bands presented in this work does not reflect the electronic coupling between the states directly involved in electron transfer, a further study that distinguishes couplings between B and H on different sides could be conducted to give some insight into the nature of the difference between the two sides of the RC. There are a number of RC mutants that could be used to carry out these further studies.

Acknowledgment. We thank Steven G. Boxer for *Rb. sphaeroides*. We thank Brad Prall, Mino Yang, Tomas Mancal, Yuan-Chung Cheng, Edward A. Berry, LiShar Huang, and Ning G. Pon for valuable discussions. This work was supported by the Office of Basic Energy Sciences, Chemical Sciences Division, U.S. Department of Energy (Contract DE-AC03-76SF000098).

References and Notes

(1) Fleming, G. R.; van Grondelle, R. *Phys. Today* **1994**, *47*, 48.
(2) Parson, W. W. Photosynthetic bacterial reaction centers. In *Protein Electron Transfer*; Bendall, D. S., Ed.; BIOS Scientific Publishers Ltd.: Oxford, 1996; p 125.
(3) Blankenship, R. E. *Molecular Mechanisms of Photosynthesis*; Blackwell Science: Oxford, 2002.
(4) Ermler, U.; Fritzsh, G.; Buchanan, S. K.; Michel, H. *Structure* **1994**, *2*, 925.
(5) Knapp, E. W.; Fischer, S. F.; Zinth, W.; Sander, M.; Kaiser, W.; Deisenhofer, J.; Michel, H. *Proc. Natl. Acad. Sci. U.S.A.* **1985**, *82*, 8463.
(6) Knapp, E. W.; Scherer, P. O. J.; Fischer, S. F. *Biochim. Biophys. Acta* **1986**, *852*, 295.
(7) Lathrop, E. J. P.; Friesner, R. A. *J. Phys. Chem.* **1994**, *98*, 3056.
(8) Scherer, P. O. J.; Fischer, S. F. *Chem. Phys.* **1989**, *131*, 115.
(9) Raja, N.; Reddy, S.; Kolaczkowski, S. V.; Small, G. J. *J. Phys. Chem.* **1993**, *97*, 6934.
(10) Plato, M.; Mobius, K.; Michel-Beyerle, M. E.; Bixon, M.; Jortner, J. *J. Am. Chem. Soc.* **1988**, *110*, 7279.
(11) Won, Y.; Friesner, R. A. *J. Phys. Chem.* **1988**, *92*, 2208.
(12) Breton, J. *Biochim. Biophys. Acta* **1985**, *810*, 235.
(13) Arnett, D. C.; Moser, C. C.; Dutton, P. L.; Scherer, N. F. *J. Phys. Chem. B* **1999**, *103*, 2014.
(14) King, B. A.; Stanley, R. J.; Boxer, S. G. *J. Phys. Chem. B* **1997**, *101*, 3644.
(15) Kirmaier, C.; Holten, D. *Photosynth. Res.* **1987**, *13*, 255.
(16) Hasegawa, J.; Ohkawa, K.; Nakatsuji, H. *J. Phys. Chem. B* **1998**, *102*, 10410.
(17) Thompson, M. A.; Zerner, M. C. *J. Am. Chem. Soc.* **1991**, *113*, 8210.
(18) Parson, W. W.; Warshel, A. *J. Am. Chem. Soc.* **1987**, *109*, 6152.
(19) Jordanides, X. J.; Scholes, G. D.; Fleming, G. R. *J. Phys. Chem. B* **2001**, *105*, 1652.
(20) Steffen, M. A.; Lao, K.; Boxer, S. G. *Science* **1994**, *264*, 810.
(21) Moore, L. J.; Boxer, S. G. *Photosynth. Res.* **1998**, *55*, 173.
(22) Jonas, D. M.; Lang, M. J.; Nagasawa, Y.; Joo, T.; Fleming, G. R. *J. Phys. Chem.* **1996**, *100*, 12660.
(23) Haran, G.; Wynne, K.; Moser, C. C.; Dutton, P. L.; Hochstrasser, R. M. *J. Phys. Chem.* **1996**, *100*, 5562.
(24) Stanley, R. J.; King, B.; Boxer, S. G. *J. Phys. Chem.* **1996**, *100*, 12052.
(25) Prall, B. S.; Parkinson, D. Y.; Yang, M.; Ishikawa, N.; Fleming, G. R. *J. Chem. Phys.* **2004**, *120*, 2537.
(26) Yang, M.; Fleming, G. R. *J. Chem. Phys.* **1999**, *110*, 2983.
(27) Mancal, T.; Fleming, G. R. *J. Chem. Phys.* **2004**, *121*, 10556.
(28) Goldmsith, J. O.; Boxer, S. G. *Biochim. Biophys. Acta* **1996**, *1276*, 171.
(29) Joo, T.; Jia, Y.; Yu, J.-Y.; Lang, M. J.; Fleming, G. R. *J. Chem. Phys.* **1996**, *104*, 6089.
(30) Agarwal, R.; Prall, B. S.; Rizvi, A. H.; Yang, M.; Fleming, G. R. *J. Chem. Phys.* **2002**, *116*, 6243.
(31) Prall, B. S.; Parkinson, D. Y.; Fleming, G. R. *J. Chem. Phys.* **2005**, *123*, 054515.
(32) Yang, M.; Ohta, K.; Fleming, G. R. *J. Chem. Phys.* **1999**, *110*, 10243.
(33) Yang, M.; Fleming, G. R. *J. Chem. Phys.* **1999**, *111*, 27.
(34) Xu, Q.-H.; Scholes, G. D.; Yang, M.; Fleming, G. R. *J. Phys. Chem. A* **1999**, *103*, 10348.
(35) Vaswani, H. M. A theoretical and femtosecond spectroscopic investigation of energy transfer in photosynthetic complexes. University of California, Berkeley, 2005.
(36) Yang, M.; Fleming, G. R. *J. Chem. Phys.* **2000**, *113*, 2823.
(37) Breton, J.; Martin, J.-L.; Fleming, G. R.; Lambry, J.-C. *Biochemistry* **1988**, *27*, 8276.
(38) Chan, C.-K.; DiMagno, T. J.; Chen, L. X.-Q.; Norris, J. R.; Fleming, G. R. *Proc. Natl. Acad. Sci. U.S.A.* **1991**, *88*, 11202.
(39) Du, M.; Rosenthal, S. J.; Xie, X.; DiMagno, T. J.; Schmidt, M.; Hanson, D. K.; Schiffer, M.; Norris, J. R.; Fleming, G. R. *Proc. Natl. Acad. Sci. U.S.A.* **1992**, *89*, 8517.
(40) Fleming, G. R.; Martin, J.-L.; Breton, J. *Nature* **1988**, *333*, 190.
(41) Jackson, J. A.; Lin, S.; Taguchi, A. K. W.; Williams, J. C.; Allen, J. P.; Woodbury, N. W. *J. Phys. Chem. B* **1997**, *101*, 5747.
(42) Jia, Y.; DiMagno, T. J.; Chan, C.-K.; Wang, Z.; Du, M.; Hanson, D. K.; Schiffer, M.; Norris, J. R.; Fleming, G. R.; Popov, M. S. *J. Phys. Chem.* **1993**, *97*, 13180.
(43) Jia, Y.; Jonas, D. M.; Joo, T.; Nagasawa, Y.; Lang, M. J.; Fleming, G. R. *J. Phys. Chem.* **1995**, *99*, 6263.
(44) King, B. A.; McAnaney, T. B.; deWinter, A.; Boxer, S. G. *J. Phys. Chem. B* **2000**, *104*, 8895.
(45) Kirmaier, C.; Bautista, J. A.; Laible, P. D.; Hanson, D. K.; Holten, D. *J. Phys. Chem. B* **2005**, *109*, 24160.
(46) Lin, S.; Taguchi, A. K. W.; Woodbury, N. W. *J. Phys. Chem.* **1996**, *100*, 17067.
(47) Michel-Beyerle, M. E.; Plato, M.; Deisenhofer, J.; Michel, H.; Bixon, M.; Jortner, J. *Biochim. Biophys. Acta* **1988**, *932*, 52.
(48) Peloquin, J. M.; Williams, J. C.; Lin, X.; Alden, R. G.; Taguchi, A. K. W.; Allen, J. P.; Woodbury, N. W. *Biochemistry* **1994**, *33*, 8089.
(49) Van Brederode, M. E.; Jones, M. R.; Van Mourik, F.; Van Stokkum, I. H. M.; Van Grondelle, R. *Biochemistry* **1997**, *36*, 6855.
(50) Van Brederode, M. E.; Van Mourik, F.; Van Stokkum, I. H. M.; Jones, M. R.; Van Grondelle, R. *Proc. Natl. Acad. Sci. U.S.A.* **1999**, *96*, 2054.
(51) Van Stokkum, I. H. M.; Beekman, L. M. P.; Jones, M. R.; Van Brederode, M. E.; Van Grondelle, R. *Biochemistry* **1997**, *36*, 11360.
(52) Vos, M. H.; Breton, J.; Martin, J.-L. *J. Phys. Chem. B* **1997**, *101*, 9820.
(53) Wang, Z.; Pearlstein, R. M.; Jia, Y.; Fleming, G. R.; Norris, J. R. *Chem. Phys.* **1993**, *176*, 421.
(54) Woodbury, N. W.; Becker, M.; Middendorf, D.; Parson, W. W. *Biochemistry* **1985**, *24*, 7516.
(55) Woodbury, N. W.; Peloquin, J. M.; Alden, R. G.; Lin, X.; Lin, S.; Taguchi, A. K. W.; Williams, J. C.; Allen, J. P. *Biochemistry* **1994**, *33*, 8101.
(56) Zinth, W.; Wachtveitl, J. *Chem. Phys. Chem.* **2005**, *6*, 871.
(57) Lin, S.; Jackson, J.; Taguchi, A. K. W.; Woodbury, N. W. *J. Phys. Chem. B* **1998**, *102*, 4016.
(58) Meier, T.; Chernyak, V.; Mukamel, S. *J. Chem. Phys.* **1997**, *107*, 8759.
(59) Mukamel, S. *Principles of Nonlinear Optical Spectroscopy*; Oxford University Press: New York, 1995.

(60) Cho, M. H.; Yu, J. Y.; Joo, T. H.; Nagasawa, Y.; Passino, S. A.; Fleming, G. R. *J. Phys. Chem.* **1996**, *100*, 11944.

(61) Groot, M.-L.; Yu, J.-Y.; Agarwal, R.; Norris, J. R.; Fleming, G. R. *J. Phys. Chem. B* **1998**, *102*, 5923.

(62) Cherapy, N. J.; Shreve, A. P.; Moore, L. J.; Boxer, S. G.; Mathies, R. A. *J. Phys. Chem. B* **1997**, *101*, 3250.

(63) Nagasawa, Y.; Passino, S. A.; Joo, T.; Fleming, G. R. *J. Chem. Phys.* **1996**, *106*, 4840.

(64) De Silvestri, S.; Weiner, A. M.; Fujimoto, J. G.; Ippen, E. P. *Chem. Phys. Lett.* **1984**, *112*, 195.

(65) Bardeen, C. J.; Cerullo, G.; Shank, C. V. *Ultrafast Phenomena X*; Springer: Berlin, 1996; p 197.

(66) Johnson, S. G.; Tang, D.; Jankowiak, R.; Hayes, J. M.; Small, G. J. *J. Phys. Chem.* **1990**, *94*, 5849.

(67) Cheng, Y. C.; Lee, H.; Fleming, G. R. *J. Phys. Chem. A*, submitted.